be recognizable by any surgeon. We report the results of reviewing FSs performed in the last 12 months at our hospital.
Design: A computer search of all FSs performed during the last 12 months (7/08 to 6/09) was conducted on a monthly bases for our QA review. We examined all pathology reports, and pertinent clinical history provided. The FSs were deemed appropriate according to the criteria mentioned above. FSs that seemed inappropriate were further investigated and were discussed with the requesting physician if needed. If there was no justifiable reason for the FS the request was categorized as inappropriate.
Results: A total of 1177 FSs were performed, of which 1165 (98.9%) were done for appropriate reasons including: 838 (71%) to establish a diagnosis for immediate treatment, 225 (19%) to assess surgical margins, and 102 (8.6%) to determine adequacy of tissue. The remaining 12 (1%) were requested for inappropriate reasons. In 5 of these when the FS diagnosis was called the surgery had already finished and the surgeon could not be located. In 7 cases the surgeons confirmed that nothing else would have been done based on the result of the FS. Five of these were done after hours or on weekends. Three surgeons accounted for 11/12 cases. They were personally contacted by the Director of the service and appropriateness of the FS request was discussed with them. Monitoring to assess whether the meetings were effective in correcting utilization of FSs is underway.
Conclusions: FS requests need to be monitored in each institution to identify inappropriate utilization and provide opportunities for education of surgeons with the aim of improving patient care, avoiding misuse of fresh tissue, and encouraging optimal expenditure of resources.

1885 "Pay for Performance" in Pathology – *Does It Perform?*

A Vora, B Feltmann, J Pfeifer. Washington University, St. Louis, MO.
Background: Pay for Performance (P4P) is a new measure instituted by the Centers for Medicaid and Medicare (CMS) in response to patient quality issues identified by the Institute of Medicine (IOM). The P4P system links compensation by CMS to measures of work quality, including improvements in patient care and pathology reporting. Per CMS, a financial incentive awarded to providers for the P4P program will result in improved patient care. However, no long-term studies have been performed in pathology to see if P4P benefits patients or their health care institutions. To address these issues, a retrospective audit was performed to determine the impact of P4P measures on patient care and financial reimbursement at our institution.
Design: A retrospective review of all breast carcinoma resections diagnosed by an academic pathology department at a tertiary care hospital was performed for fiscal year (FY) 2008 (June 2007-July 2008). Based on the pathology reports, resections were stratified to see if they met or exceeded defined P4P criteria, and the resulting professional and administrative costs of implementing the P4P algorithm were calculated.
Results: Of the breast carcinoma resections in FY 2008 (n=1,252), only 25% (n=319) were patients covered by the Medicare program; 100% of these cases met the inclusion criteria for P4P best medical practice and the performing pathologist's total Medicare allowable charge base was $290,239. The calculated P4P bonus on these charges was $4,354 (1.5% of the allowable charges). However, the retrospective analysis demonstrated that it had cost $5,870 to implement the changes in specimen processing and reporting to meet P4P criteria, and that there was a $330 administrative cost involved in submission of P4P claims. A similar analysis of colon adenocarcinoma resections showed that 100% of cases met inclusion criteria for P4P best medical practice, but that the costs of participation in the P4P program exceeded the reimbursement received (data not shown).
Conclusions: In a tertiary care academic pathology department, participation in the P4P program did not improve patient care (standard of care reporting criteria in the department met or exceeded P4P criteria in 100% of breast and colon resections prior to participating in the P4P program). Furthermore, the P4P algorithm did not provide a clear financial incentive (participation in the P4P program was associated with a net cost). We conclude that, in the setting of a tertiary care academic pathology department, patient care needs dictate reporting standards, not P4P initiatives.

Pan-genomic/Pan-proteomic Approaches to Diseases

1886 Derivation and Independent Validation a Gene Expression-Based Predictor for Post-Cystectomy Recurrence in Nodal Negative Muscle Invasive Urothelial Carcinoma

AS Baras, SC Smith, CA Moskaluk, HF Frierson, D Theodorescu. UVA Health System, Charlottesville, VA.
Background: Despite radical surgery and lymphadenectomy, approximately half of muscle invasive urothelial carcinoma (MIUC) patients experience metastatic recurrence within two years of surgery. Within this population, patients with nodal negative disease are not commonly offered adjuvant chemotherapy, though treatment failures remain common. Predictive risk stratification in this population would be useful for decisions regarding adjuvant therapy.
Design: We used two published studies of gene expression profiling of tumor tissue to design a prediction metric for recurrence post-cystectomy among pathologically node negative MIUCs. First, we used one dataset based on the Affymetrix HG-U133A platform for training to compare gene expression between a subset of cases evincing disease free survival >2 years (N=17) to those with disease specific recurrence in < 2 years (N=14). A nearest neighbor classification system yielding a prediction score from 0 to 1 was employed to classify samples based on expression of recurrence related genes. This gene set was then applied to an independent test dataset of 47 tumors profiled on the Illumina Human WG6 V2 platform. Association between the gene expression-based prediction score and clinicopathologic parameters was tested through multivariate logistic regression and receiver operating characteristic (ROC) analysis.
Results: By a criterion of 2-fold differential expression, > 75 units average difference, and P<0.001, we found 33 candidate probes associated with disease recurrence in the training set. Prediction scores within the learning dataset were found to be independent of stage, grade, age, and sex (p=0.011). From these 33 probes, 27 Unigene IDs were able to be matched across microarray platforms. When the same prediction algorithm was applied to the independent test set of nodal negative MIUCs, we again found a significant independent association with disease recurrence (P=0.015), with a favorable area under the ROC curve (P=0.012).
Conclusions: Prediction models derived from gene expression analysis of tumor tissue samples can provide independent prognostic information about the course of patient disease in node negative stage MIUCs. This approach may show promise as an adjunct to routine histologic examination in determining patient therapy, pending validation in larger independent cohorts.

1887 Gene Set Enrichment Analysis Identifies Ovarian Tumor Field Defect

J Cuff, AH Beck, TA Longacre. Stanford University, Stanford, CA.
Background: Ovarian endometrioid and clear cell carcinoma are associated with endometriosis. A step-wise transformation of a specific precursor lesion has been proposed for clear cell carcinoma, while a possible field defect has been postulated for endometrioid carcinoma, whereby neoplastic progression is distributed throughout the extended mullerian system. We utilized gene set enrichment analysis to determine whether unique patterns of gene expression in ovarian clear cell and endometrioid carcinomas are distinct with regard to endometriois, an acknowledged common precursor lesion.
Design: We pursued a two step bioinformatic approach utilizing publicly available gene expression data. Significance analysis of Microarray's (SAM) was used to construct an endometriosis gene signature by comparing expression array data **(GSE7305)** from endometriosis (n=10) and cycling eutopic endometrium (n=10). SAM was implemented in R where ~1000 probes were deemed to be significantly different between the two groups (delta level =5; false discovery rate of zero expected at this level of significance). The second step utilized a data set of stage I ovarian cancers (GSE8841); analysis was restricted to the subset of clear cell and endometrioid carcinomas (n=35). Gene Set Enrichment Analysis (GSEA; Broad institute) was performed to determine if differences in gene expression between clear cell and endometrioid carcinomas differ in a coordinated fashion with respect to the previously defined background/stromal gene expression of endometriosis.
Results: A set of 36 genes was upregulated in endometriosis and significantly enriched in endometrioid but not clear cell carcinoma. Gene annotation revealed several known oncogenes, genes encoding tyrosine kinases, and genes associated with neoplasia inducing translocations. These genes are suspect candidates in the neoplastic transformation of a common precursor lesion into distinct tumor types.

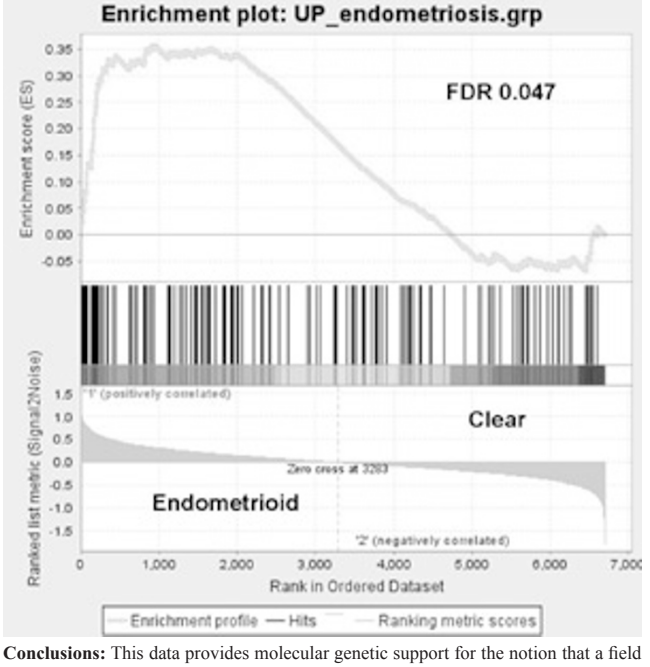

Conclusions: This data provides molecular genetic support for the notion that a field defect with a unique set of genetic changes is operative in ovarian endometrioid but not clear cell tumors. Endometriosis may presage ovarian endometrioid and clear cell carcinoma, however different genetic changes likely participate in divergent morphologic and clinical phenotypes.

1888 Proteomic Analysis of Barrett's Associated Neoplasia Identifies Protein Markers Correlating with Neoplastic Progression

JM Davison, MS Flint, BL Hood, BA Jobe, TP Conrads. U of Pittsburgh Med Ctr, Pittsburgh, PA.

Background: Barrett's esophagus (BE) is a major risk factor for the development of esophageal adenocarcinoma (AdCA), a clinically aggressive malignancy which has dramatically increased in incidence during the past 20-30 years. The fact that >90% of patients with adenocarcinoma are discovered when the adenocarcinoma is advanced underscores the need for more effective identification of people who are at risk. Protein biomarkers associated with neoplastic progression from BE to AdCA may facilitate diagnosis.

Design: We harvested formalin-fixed paraffin-embedded tissues from 14 esophagectomy specimens and analyzed 10 samples of BE, 11 samples of high grade columnar dysplasia (HGD) and 10 samples AdCA. Epithelium and surrounding stroma were obtained by laser capture microdissection. Approximately $6x10^6$ um^2 of tissue (approximately 20,000 cells estimated) was collected for each sample. Tissue was then and analyzed in duplicate by nanoflow LC-MS/MS. The primary tandem MS data were searched against the human proteome database (UniProt) for peptide identification and subsequently analyzed to identify unique peptides. A protein's spectral count (i.e., the number of sequenced peptides per protein) served as a quantitative estimate of the abundance of proteins in a sample.

Results: 1. Over 2000 unique peptides were identified per LC-MS/MS analysis of 20,000 cells on column with an average relative standard deviation (RSD) of peptide identification rate of 15% across all injections, and an average of nearly 700 proteins identified per tissue sample. 2. Over 350 proteins showed significant differences in abundance between BE, HGD and AdenoCA tissue sample sets (Kruskal-Wallace non-parametric ANOVA with $p < 0.05$). 3. A supervised hierarchical cluster analysis incorporating proteins with significant differences in abundance correctly classified 10/10 BE samples, 10/11 HGD and 9/10 AdCA samples and showed patterns of relative protein abundance to correlate with tissue diagnosis. 4. This approach identified expected declines in abundance of CK20, MUC-5AC and MUC-2 between BE, HGD and AdenoCA. Proteins involved in signal transduction, cell cycle regulation, cell growth and differentiation, angiogenesis, matrix remodeling, cell motility, among other functions showed gradients of abundance between sample sets.

Conclusions: Mass spectrometric analysis of small samples of formalin-fixed tissue is capable of identifying gradients of protein abundance between BE, HGD and AdenoCA which are of likely biologic relevance in neoplastic progression.

1889 Viral Insertion Site Discovery Using Next Generation Sequencing of Formalin Fixed Tissue

EJ Duncavage, JR Armstrong, VJ Magrini, N Becker, R Demeter, ER Marids, JD Pfeifer. University of Utah, Salt Lake City, UT; Washington University, Saint Louis, MO.

Background: Many techniques exist for mapping viral integration sites. However, these methods require large intact stretches of DNA and none is ideally suited for DNA extracted from formalin-fixed paraffin-embedded (FFPE) tissue. We present data mapping Merkel cell polyomavirus (MCPyV) genome integration sites from FFPE tissue using a novel method that combines hybrid capture, Illumina sequencing, and bioinformatics.

Design: First, viral capture probes covering the entire 5.3kb MCPyV genome were constructed by designing 23 overlapping, 275 bp long, PCR products; biotin-labeled dCTP was incorporated into the amplicons during the PCR amplification (the PCR products were sequence verified and biotin incorporation was confirmed). Second, we identified four cases of MCC that harbored MCPyV as confirmed by PCR, and extracted genomic DNA from cores of FFPE tumor tissue; the DNA was analyzed for quality/quantity and modified for Illumina sequencing. Third, the genomic DNA was hybridized with the biotinylated capture probes at 71°C for 48 hours in the presence of Cot-1 DNA; streptavidan-labeled paramagnetic beads were then added to the hybridization mixture and the hybridized DNA 'pulled-down' by a magnet. Fourth, the captured tumor DNA was melted away from the bead-bound amplicons and sequenced on an Illumina GAII analyzer using 50bp, or 75bp paired-end reads. The resulting data were aligned to the MCPyV viral genome, and chimeric viral/human sequences representing viral integration sites identified.

Results: Viral integration sites were correctly identified in 3 of 3 cases sequenced with 75bp reads. A definitive insertion site could not be identified in cases sequenced with shorter non-paired reads. Coverage of the viral genome ranged from 4,000x to 36,000x, with a minimum viral sequence enrichment of 30,000 fold.

Conclusions: Viral integration sites can be identified from FFPE tissue even if the viral insertion sequence is unknown. However, 75bp or longer reads are required to produce chimeric sequences informative enough to identify integration sites. This methodology could easily be applied to elucidate other chimeric DNA sequences from FFPE, such as identification of translocations where one partner gene is unknown.

1890 Use of Computer Assisted Analysis To Facilitate Tissue Microarray Interpretation

L Goodell, W Chen, P Javidian, M Chekmareva, J Hu, DJ Foran. UMDNJ-Robert Wood Johnson Medical School, New Brunswick, NJ.

Background: Tissue microarrays (TMA) have surged in popularity as a tool to conserve human tissue in translational research. Interpretation of TMAs, often with hundreds of tissue cores, is tedious. Our group has developed algorithms and conducted man-machine comparison studies to evaluate the use of computer assisted analysis to facilitate standardization, semi-quantitative interpretation and management of biomarker data using immunohistochemistry (IHC).

Design: Man-machine concordance studies were designed to evaluate IHC staining intensity on 5 breast cancer TMA slides stained with CK18, Her2, Cyclin D1, CK19 and ER digitized using a Trestle MedMicroscopy system at 40x equivalent resolution. Automatic quantification algorithms analyze the color profiles of each specimen, decompose the histospots into constituent staining maps according to the Principle Color Vectors, and generate Effective Staining Intensity (ESI) scores. Using our TMR software, a pathologist first selected representative histospots of different semi-quantitative staining levels for standardization. Three pathologists then used the TMR software [Figure 1] to evaluate each tissue disc by selecting a staining level or rejecting the image based upon the tissue quality and image fidelity using a standard set of controlled lighting/viewing conditions. The ESI scores were mapped back to the same evaluation categories used by the pathologists through linear regression.

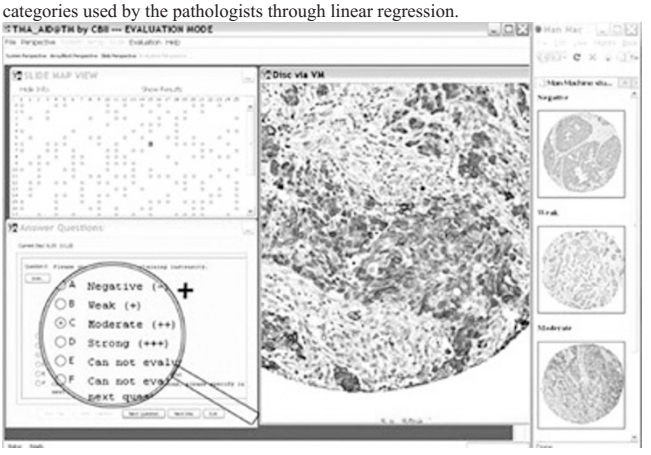

Results: Concordance between pathologists and computer scores were measured from 1407 tissue cores using squared-weighted Cohan's kappa to account for the ordinal nature of the grading scale (Table 1).

TMA Man-Machine Correlation

TMA slide	Inter-Pathologist		Computer-pathologist	
	κ	correlation	κ	correlation
CK 18	.89	.90	.82	.84
Her2	.75	.78	.81	.84
Cyclin D1	.84	.85	.78	.78
CK19	.85	.86	.84	.84
ER	.81	.82	.77	.79

Conclusions: Results show the computer algorithms achieved similar concordance to interpretations by experienced pathologists and were consistent with inter-pathologist concordance. Future studies will focus on optimization of algorithms and standardization of IHC staining to support high throughput TMA analysis.

1891 Piwil2-Like Proteins Are Expressed in Precancerous Stem Cells and Various Types of Cancers and Can Regulate Tumor Development

G He, RL Shen, Q Zhou, L Chen, Y Ye, C Shapiro, SH Barsky, JX Gao. Ohio State University, Columbus, OH; Soochow University, Suzhou, Jiangsu, China.

Background: Piwil2, a member of AGO/PIWI family proteins, which is silenced in adult tissues has been implicated to play an important role in tumor development. However, the mechanism underlying piwil2 regulating tumor development is largely unknown. Our previous studies have suggested that piwil2-like (PL2L) proteins might regulate precancerous stem cell (pCSCs) development. Herein, we demonstrated that PL2L proteins are expressed in various types of cancers and can regulate tumor development.

Design: First, piwil2-specific Gene-Exon-Array (GEA) RT-PCR was developed to determine the existence of piwil2-like (PL2L) protein transcripts. Then, bioinformatics was used to design a peptide shared by piwil2 and PL2L proteins, which was used to generate polyclonal (pAbs) and monoclonal antibodies (mAbs). Both pAbs and mAbs are able to recognize full length piwil2 and at least four PL2L proteins of human and mouse, including PL2L80, PL2L60, PL2L50, and PL2L40. By using the unique antibodies, we investigated the function of PL2L proteins in tumor developments and their clinic-pathological significance.

Results: A number of piwil2-like (PL2L) proteins, including PL2L80, PL2L60, PL2L50, and PL2L40 have been identified by monoclonal antibodies (mAbs) to piwil2 peptides. Especially, PL2L60 is dominantly and widely expressed in pCSCs and tumor cell lines without the restrictions of tissue origin. The PL2L60 mediated pCSC and tumor cell expansion *in vitro* is associated with up-regulation of Stat-3 and Bcl-2 genes. Immunohistochemical analysis has revealed that PL2L proteins, rather than piwil2, are ubiquitously expressed in various stages of human primary and metastatic cancers. While PL2L proteins are associated with cancer cell proliferation, piwil2 expression is associated with cancer cell apoptosis.

Conclusions: These findings suggest that piwil2 and PL2L proteins might play important but opposite roles in tumor development and that PL2L proteins might have the potential to be used as a common biomarker for diagnosis, prognosis and effective therapeutic target in early stage of the human cancers.

1892 Detecting Phenotypical Subtypes of Breast Cancer with Multiplexed Immunohistochemistry

C Hoyt, J Rheinhardt, N Torsten, H Gardner. Cambridge Research & Instrumentation, Inc., Woburn, MA; Novartis Institutes for Biomedical Research, Cambridge, MA; British Columbia Cancer Agency, Vancouver, BC, Canada.

Background: Treatment for breast cancer has benefited significantly from advances in molecular biology. IHC tests for protein receptors ER, PR, and Her2 have lead to a new patient classification system – Luminal A (ER+, PR+, and Her2-), Luminal B

(reduced ER or PR percent positivity), Her2-positive, and Basel-like (ER-, PR-, Her2-). Traditional approaches to assessing multiple proteins use serial sections, staining for one protein per serial section. If multiple proteins are assessed in the same tissue section, co-expression can be detected on a per-cell basis. Percent double and triple positivity can be assessed, possibly revealing significant subtypes and leading to more targeted and more effective treatments and therapies.

Design: Having previously developed: a) multi-label immunohistochemical staining methods; b) an automated multispectral slide analysis system; and c) image analysis algorithms to differentiate relevant tissue regions (e.g., tumor vs stroma and necrosis, etc.) and to segment cellular compartments, the goal is now to perform pilot studies using archived clinical material, to determine whether per-cell co-expression subtypes can be uncovered.

Results: Multispectral imaging was performed on two sets of a 712-core TMA (356 patients represented in duplicate). The first set was stained for ER and ki67 plus counterstain, and the second for ER, PR and Her2, plus counterstain. IHC signals were spectrally 'unmixed' from each other and counterstain. Machine-learning-based automated image analysis was performed to locate cancer cells, segment subcellular compartments, and extract IHC signals on a per-cell basis. Per-cell co-expression subtypes were detected using flow-cytometry data analysis software. Each TMA core was imaged and processed at a rate of about three cores per minute. Image analysis algorithms were trained in under 2 hours, and then used to process core images at approximately 10 seconds per core. Percent double and triple positivity were determined, revealing subtypes. Correlation between subtypes and clinical outcomes will be the topic of future publications.

Conclusions: Together, the innovative multispectral platform and image analysis software, coupled with flow-cytometry analysis tools, sometimes termed 'tissue cytometry', can be used to reveal molecular subtypes, which may lead to new targeted strategies for breast cancer research and clinical care.

1893 Aberrant Expression of pRb and p16^{INK4A} Proteins in Non-Squamous Non-Small Cell Lung Cancer (NSCLC) and Their Relationship with Patient Survival: A Retrospective Cohort Study

CC Huang, M Leon, C Elkins, CJ Yao, Y Li, K Gibson, G He, G Otterson, M Villalona, Y Tang, WQ Zhao. Ohio State Unversity Medical Center, Columbus, OH; South Center University, The 3rd Xiang-Ya Medical School, Changsha, Hunan, China; Ohio State University Medical Center, Columbus, OH.

Background: Deregulation of several genes involved in cell cycle control has been reported in Non-Small cell lung cancer (NSCLC). The protein expression of p16^{INK4A}, pRb, p53 and the copy number alterations of *CDKN2A* gene in NSCLC and their association with patients' survival were investigated.

Design: 73 NSCLC (M:43, F:30) (median age=65.5) at stage IA to IIB were enlisted in this study. A TMA was built on the FFPE tissues. The IHC for p16^{INK4A}, pRb, and p53 were performed and scored as negative (0), low (1+), and high (2+ and 3+). The FISH for *CDKN2N(p16)* gene was performed on the TMA and/or on FFPE tissues. The ratio of gene copy numbers (CPN) to centromere (CEP9) was calculated. The CPN were expressed as normal (ratio of 1), heterozygous loss (0.5), hemizygous loss (0), polysomy (>6 copies but ratio<2), and amplification (>2.1). The five-year absolute survival rate after the diagnosis was used.

Results: The majority of cases were adenocarcinoma (69.9%). p16^{INK4A} protein was correlated significantly with CPN of *p16* (p=0.0007). Higher p16^{INK4A} expression was observed in 30% cases. Overexpression of p16^{INK4A} with either *p16* amplification or polysomy was associated with a poor prognosis (OR 7.519, 95% CI 1.106-15.521, p=0.009). In cases with negative p16^{INK4A} IHC, 74.5% cases had a normal CPN, and were not correlated with survival (p>0.05). However, among those p16^{INK4A} negative cases, the lower pRb expression was associated with a longer survival (86%, 24/28) which was significantly different from those with a shorter survival (30%, 7/23) (p<0.0001). Furthermore, without considering p16^{INK4A} status, overexpression or no expression of pRb made up to 60% and 27.5%, respectively, of the patients with a shorter survival (n=40); which was significantly higher than those with longer survival in which only 16.7% and 6.7% (p<0.001) had over- or none expression. Therefore, the pRb expression alteration was an independent predictor for poor survival.

Conclusions: The overexpression of p16^{INK4A} with either *CDKN2N(p16)*amplification or polysomy was associated with a poor prognosis. Higher pRb expression in p16^{INK4A} negative NSCLC cases was also associated poor prognosis.

1894 Molecular Subtyping of Lung Cancer in Smokers and Never-Smokers: A Subset of Adenocarcinomas Characterized by *ASCL1* Expression

CM Ida, MC Aubry, P Yang, F Kosari, G Vasmatzis. Mayo Clinic, Rochester, MN.

Background: Gene expression profiling represents a powerful tool to unravel tumor molecular heterogeneity underlying different clinical outcomes of tumors with similar histology and clinical stage, especially amongst non-small-cell lung cancer subtypes. Smoking is a well-established risk factor implicated in lung carcinogenesis. Different tumor molecular pathways seem to be operating in smokers (S) and never-smokers (NS). We performed gene expression profiling to differentiate molecular subtypes in lung cancers.

Design: Frozen lung tumor tissue samples from S and NS were used.

Lung cancer subtype/ Smoking status	SMOKERS (n=209)	NEVER-SMOKERS (n=261)
ADENOCARCINOMA	135	90
SQUAMOUS CELL CARCINOMA	25	3
ADENOSQUAMOUS CARCINOMA	2	6
SMALL CELL LUNG CARCINOMA	14	-
LARGE CELL CARCINOMA	10	5
CARCINOID TUMOR	-	32
PNEUMOCYTES	23	125

Clinical staging and follow-up information was obtained for all patients. Gene expression datasets were generated using microarray technology. For S and NS, unsupervised analysis using a group of differentiation genes assessed molecular clustering and histopathological classification correlation, and Kaplan-Meier curves were generated to evaluate survival.

Results: In S (**A**) and NS (**B**), tumors clustered in groups that recapitulate histopathological classification.

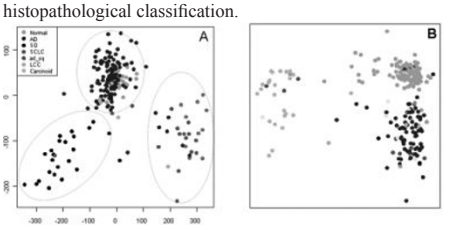

Amongst adenocarcinoma (AD), *ASCL1,* a lung neuroendocrine (NE) differentiation gene, was expressed by a subset of AD (*ASCL1*+AD). *ASCL1*+AD was present in 25% of AD in S and 4% of AD in NS,(p=0.0012). Preliminary survival analysis indicates less favorable outcome for *ASCL1*+AD, particularly in stage I disease (**C**).

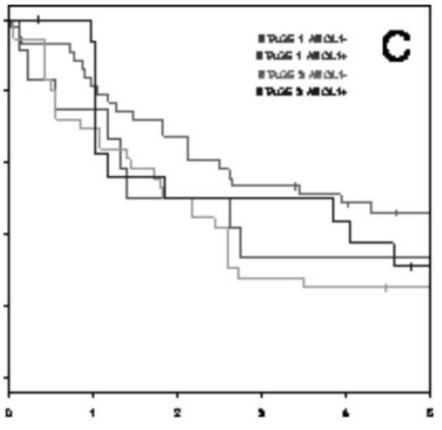

Conclusions: We confirmed gene expression profiling as a robust ancillary method to subtype lung cancer molecularly in both S and NS. We showed that a subset of AD express the NE-related gene *ASCL1.* These were more frequent among S and were associated with less favorable outcome in stage I disease.

1895 Topoisomerase II alpha Protein Expression Is Predictive of Outcome in Gleason Score ≥ 7 Prostate Cancer Patients Treated Surgically and Is Dependent on *ERG* Status

CM Ida, JC Cheville, RJ Karnes, JM Munz, G Vasmatzis. Mayo Clinic, Rochester, MN.

Background: Recently, a prognostic model for high Gleason Score (GS) prostate cancer (GS ≥7) consisting of gene expression of *TOP2A* and *CDH10, TMPRSS2-ERG* fusion and DNA ploidy was described. Topoisomerase II alpha gene (*TOP2A*), which encodes an enzyme involved in DNA replication, was the strongest predictor of outcome. *TMPRSS2-ERG* fusion is a frequent recurrent abnormality believed to represent an early event in prostate carcinogenesis. It results in *ERG* gene overexpression and its association to tumor aggressiveness is controversial. We evaluated the prognostic value of TOPO2A protein expression in comparison to *TOP2A* mRNA expression in GS ≥7 prostate cancer in the context of *ERG* status defined by high (*ERG+)* or low (*ERG-)* mRNA expression.

Design: GS ≥7 patients that developed systemic progression or died of prostate cancer within 5 years following surgery (n=140, cases) and patients free of disease within at least 7 years of follow-up (n=117, controls) were identified. A computerized score combining GS, margin status and preoperative serum PSA, was used to match cases and controls. *ERG* and *TOP2A* mRNA levels were measured by qRT-PCR. TOP2A protein expression was assessed by immunohistochemical (IHC) analysis and quantified using IHC Score Software (Bacus Laboratories, Inc.) to obtain TOP2A labeling indices (LIs).

Results: TOP2A LIs mean±SD for cases and controls were 3.45±5.18 (range, 0.02-30.74) and 0.92±1.34 (range, 0.01-7.09), respectively (p⟨0.001). In addition, TOP2A protein expression was a superior prognostic indicator than *TOP2A* gene expression (AUC 0.75 for IHC analysis *vs*. 0.70 for qRT-PCR). Notably, the prognostic ability of TOP2A IHC was dependent upon the *ERG* status. In *ERG-* prostate cancer, TOP2A IHC was a stronger predictor of outcome (AUC 0.81 for *ERG- vs*. AUC 0.67 for *ERG+*).

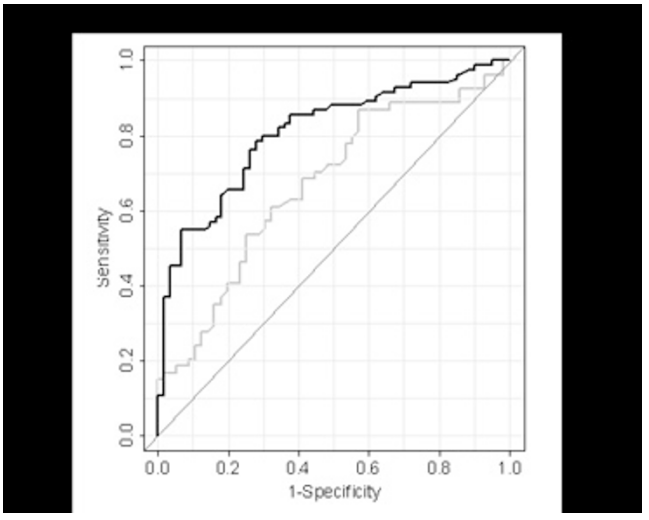

Conclusions: TOP2A IHC protein expression by immunohistochemistry was predictive of systemic progression and death in patients with GS ≥7 prostate cancer treated surgically, especially in prostate cancer without *ERG* overexpression. Therefore, TOP2A protein expression is a potential prognostic predictor to individualize postoperative therapy based on risk of systemic progression.

1896 The Effect of Hollande's Fixative on the mRNA Levels in Normal Pancreas

DK Kaneshiro, Y Jiang, Y Wang, X Liu. Cleveland Clinic, Cleveland, OH; A Johnson & Johnson Company, San Diego, CA.

Background: Buffered neutral formalin (BNF) is a widely used fixative in histology laboratories and is considered suitable for preservation of both DNA and RNA for molecular studies. Hollande's solution is also a commonly used fixative; however, its effects on mRNA levels have not been previously reported. This study aims to retrospectively determine mRNA levels for 3 endogenous genes [β-actin, hydroxymethylbilane synthase (HMBS), ribosomal protein L13 A (RPL13A)] and 2 additional genes [human equilibrium nucleotide transporter 1 (hENT1) and ribonucleotide reductase subunit 1 (RRM1)] in normal pancreas fixed in either Hollande's solution or BNF.

Design: Normal pancreas from 12 cases from years 2000-01 fixed using Hollande's solution, 9 cases from 2002-03 fixed using BNF, and 34 cases from 2004-05 fixed using BNF were included in the study. Unstained slides were microdissected to only include normal pancreas for RNA isolation. 100 ng total of RNA from each specimen was used for the one-step RTQ-PCR using paired primers for β-actin, HMBS, RPL13A, hENT1 and RRM1. The mRNA level was expressed by the cycle threshold (Ct) value. The results of the Hollande's fixed, BNF-fixed (2002-03) and BNF-fixed (2004-05) groups were compared using a Mann-Whitney U test, with a level of significance set to $p<0.05$. The mRNA level difference between groups was expressed for each gene by ΔCt and the fold (%) calculated using the formula $(1/2^{\Delta Ct})$ x 100%.

Results: See Table 1 for results.

mRNA Levels of β-actin, HMBS, RPL13A, hENT1 and RRM1 in Normal Pancreas Fixed in Hollande's and BNF

	β-Actin	RPL13A	HMBS	hENT1	RRM1
Hollande's (N=12, 2000-01)	23.82	24.84	31.33	29.22	30.90
BNF (N=9, 2002-03)	21.89	22.27	29.68	25.99	28.26
BNF (N=34, 2004-05)	21.65	22.38	29.72	26.42	28.46
P value Hollande's vs BNF (2002-03)	0.0018	0.0072	0.0092	0.0117	0.0014
P value Hollande's vs BNF (2004-05)	0.0016	0.0013	0.0022	0.0059	0.0015
P value BNF (2002-03) vs BNF (2004-05)	0.368	0.243	0.323	0.965	0.693
Fold (%) [Hollande's/BNF (2002-03)]	14.53	7.64	19.21	12.06	13.85
Fold (%) [Hollande's/BNF (2004-05)]	11.38	8.57	19.84	18.44	16.55

Conclusions: Hollande's fixative significantly decreases the mRNA levels in normal pancreas.

1897 Analysis of Microarray Data from High Grade Gliomas across Multiple Institutions

S Le, S Sanga, BM Broom, K Aldape, V Cristini, ME Edgerton. MD Anderson Cancer Center, Houston, TX; University of Texas at Austin, Austin, TX.

Background: We combined gene expression data from HGG's from M.D. Anderson Cancer Center, Henry Ford Hospital, and University of California, Los Angeles (UCLA) and performed a series of data mining experiments to identify causative gene networks that contribute to aggressive behavior in High Grade Glioimas (HGG).

Design: Data was normalized and divided into class 1 (survival of less than 30 weeks from date of diagnosis) and class 2 (survival of greater than 125 weeks from date of diagnosis). Two-thirds of the data were used as a training set and remaining one-third as a test set, each with approximately 72% class1 and 28% class 2 patients. We used SAM to select for genes and constructed a vote based model to predict class. We performed 2-D hierarchical clustering (HC) to determine which rules clustered with accurate predictions on which patient set. Metacore was used to search for functional relationships and common transcription factors.

Results: We achieve acceptable accuracy (80%) with a set of 117 genes from SAM. The rules defined by SAM genes generate three clusters, one for class 2 (good prognosis) and 2 for class 1 (poor prognosis). Metacore identifies multiple functions and transcription factors associated with class 1 genes, including development, morphogenesis, kinase activity and response to hypoxia.

Conclusions: Rule analysis in combination with pathways databases can be used to study interactions in molecular profiles in HGG, which partition into two poor and one good prognosis molecular subtypes. Genes upregulated in the largest cluster of class 1 and most closely networked share multiple transcription factors, including GGR-alpha, c-fos, Lef1, p-53, NK-Kb, Stat1, Stat3. Stat50, PAX2, and NR2E1.

1898 High Resolution Analysis of Genome-Wide Copy Number Change in Neuroendocrine Carcinoma of the Breast

X Leng, R Shui, L Shen, KA Baggerly, X Liu, C Liu, A Sahin, SC Abraham, Y Wu. The University of Texas M. D. Anderson Cancer Center, Houston, TX; Cancer Hospital, Fudan University, Shanghai, China.

Background: Neuroendocrine carcinoma (NEC) of the breast is an unusual subtype of breast carcinoma. Little is known about the genetic alterations involved in breast NEC.

Design: To gain a better understanding of the underlying mechanisms of breast NEC, genomic DNA were extracted from freshly collected tissues of six breast neuroendocrine carcinoma and three normal breast. The genomic DNA were labeled and hybridized to Affymetrix SNP array 6.0, which contains 946,000 probes for detection of changes in the gene copy numbers at genome-wide scale. The diagnoses of all six breast NEC cases were confirmed by immunohistochemical staining using neuroendocrine markers synaptophysin and/or chromogranin, with more than 50% of invasive tumor cells positive for one or both markers. The changes in the gene copy numbers were analyzed using **Partek** Genomic Suite software (Partek, Inc. St Louis, MO).

Results: The analyses showed that breast NEC samples displayed increased gene copy numbers in the two sets of chromosomal regions, one set contained genes invovled in neuronal or endocrinal functions (e.g. GRM8, EPHA7, prosaposin, PRIMA1, RAB27B, ACCN1, GPR337L1, ZHX2) and the other set contained genes involved in promoting cell cycle and tumorigenesis (e.g. FBXO11, DLG1, ZDHHC1, HINT1, FBXW11, DOCK5, MOS, PLAG1, FGF3, NCOA2). Accordingly, we found that chromosomal regions containing tumor suppressors (e.g. ELK3, ELAVL2, KITLG, WWOX) were deleted. Other deleted regions contained the genes involved in normal and neuronal development (e.g. CDH7, NFIB, DYNC2H1). We also detected changes in the copy numbers of a few genes with unknown function. In particular, SUSD1, a sushi domain containing protein 1, displayed increased copy numbers in all six breast NEC samples. The function of SUSD1 in breast NEC is not clear and needs further investigation.

Conclusions: A wide spectrum of genetic aberrations was identified in NEC of the breast. Additional studies will be needed to further explore the potential mechanisms in the development of breast NEC which involves the identified candidate genes from this study.

1899 The Role of mTOR/Stat3 in Tumorigenesis in Chronic Ulcerative Colitis

Q Liu, J Hart, K Tanaka, M Bissonnette, E Lin. Montefiore Medical Center of Albert Einstein College of Medicine, New York, NY; The University of Chicago Medical Center, Chicago, IL.

Background: The pathogenesis of inflammatory bowel diseases (IBD) is thought to involve modulation of the intestinal mucosal immune response determined by a complex interplay of genetic, microbial and environmental factors. However, our mechanistic understanding of the link between inflammation and tumorigenesis in the colon is limited.

Design: This study was designed to characterize differences in gene expression in colonic mucosa between normal (n= 5 patients) and chronic ulcerative colitis (UC) patients with or with dysplasia (N=17 patients). A newly established mouse model of colitis-associated colorectal cancer, the Stat3-IKO mouse, was used to identify potential key tumor-promoting factors and determine the function of these factors identified in patients with chronic ulcerative colitis.

Results: Our studies demonstrated that mTOR/Stat3 pathway was activated in colonic epithelial cells in both human chronic colitis (UC) and the mouse model. Using the mouse model of colitis-associated colorectal cancer, we found that activation of mTOR/Stat3 pathway is specifically induced by inflammation and was associated with disruption of colonic homeostasis, fulminant epithelial/tumor cell proliferation and tumorigenesis in the inflamed colon. In the colonic mucosa of patients with chronic UC and dysplasia, there is an enhanced anti-microbial reaction similar to that observed in the mouse model. Upregulation of proinflammatory cytokines, CXCL10, CXCL11 and CCL9, and a repression of IL-17 signaling was observed in the mucosa of UC patients with dysplasia elsewhere in their colon, when compared to normal mucosa or UC mucosa without dysplasia. Cytokines whose activities are mediated by CXCR3 and CCR7 were markedly up-regulated in the inflamed colonic mucosa in Stat3-IKO mice. These findings suggest that the mTOR/Stat3 pathway is important in the development of IBD and dysplasia.

Conclusions: The activation of mTOR/Stat3 pathway in colonic epithelial cells, specifically induced by inflammation, may play a critical role in promoting tumorigenesis in ulcerative colitis. Several cytokine/chemokine pathways assoicated with antimicrobial function were found abnormally regulated in both human ulcerative colitis and inflamed colon of mouse. The future study is to identify the mechanistic link between dysregulated mucosa immunity and activation of the oncogenic pathway, mTOR/Stat3.

1900 Putative Signatures Predict High-Risk Oral SCC: Feasibility of Gene Discovery Using Tumors with Limited Formalin Fixation and the DASL Platform

O Loudig, R Kim, J Segall, A Negassa, M Prystowsky, M Brandwein-Gensler. MMC/Einstein, Bronx, NY; Einstein, Bronx, NY.

Background: Our Risk Model is predictive of time to disease-progression for patients with HNSCC. Patients are classified as either low-, intermediate-, or high-risk after examining resection specimens for specific variables; a current limitation is that risk-score cannot be assigned on biopsies as their small size limits full evaluation of these variables. Identifying high-risk on biopsy could assist in planning more aggressive therapy and proper patient counseling. Our goal is to develop an RT-PCR test for formalin fixed paraffin embedded (FFPE) biopsies that is predictive of high-risk and poor-outcome. Our gene discovery approach uses tumor-enriched oral SCC samples subjected to limited FFPE. Array analysis is performed using the Illumina DASL (cDNA-mediated annealing, selection, extension and ligation) 24,000 probe assay, which is designed to detect partially degraded mRNAs as small as 50 nucleotides.

Design: Banked frozen specimens from 17 oral SCC (9 high-, 4 intermediate-, 4 low-risk) had limited FFPE (24 hours). Morphologically-guided tumor-enriched 1 mm cores were procured and mRNA extracted. The DASL platform was used for expression analysis. Raw data was analyzed without background subtraction after robust spline normalization. Standard T-test detected significant fold-change in gene expression between low- and high-risk tumors.

Results: RNA integrity index was ≥ 2.4, confirming suitability for study. Repetition of paired FFPE samples confirmed perfect reproducibility (R = 1.00). Standard T-test analysis revealed 157 genes differentially expressed in high-risk tumors with a 10% false discovery rate (FDR).

Some of these genes are involved in mitotic and signal transduction pathways; others genes regulate cell shape, polarity and migration.

Conclusions: We have demonstrated feasibility of using FFPE tumors for gene discovery and identified 157 genes (FDR 10%) that are differentially expressed in high- and low-risk oral SCC. This approach will facilitate the development of predictive RT-PCR test for routine biopsy samples.

1901 Highly Multiplexed Detection of Translocation Fusion Transcripts without Amplification Using the NanoString Platform

A Luina Contreras, S Jackson, M Ladanyi. Memorial Sloan-Kettering Cancer Center, New York, NY; NanoString Technologies, Inc, Seattle, WA.

Background: Translocation-associated gene fusions are useful diagnostic markers. Current methods of detection include fluorescent in-situ hybridization (FISH) and reverse transcriptase PCR (RT-PCR). Here, we describe the development of an assay, based on the NanoString platform, for detecting sarcoma translocations using color-coded probe pairs without any PCR amplification step.

Design: We designed a multiplex probe library for EWS-FLI1; EWS-WT1; SYT-SSX1 and SYT-SSX2; and PAX3-FKHR and PAX7-FKHR, based on paired oligonucleotide probes. RNA molecules are immobilized using a 50 nt capture probe, corresponding to the portion immediately 5' to the chimeric transcript fusion junction. The second probe, the reporter probe, is a 50 nt probe hybridizing to the portion immediately 3' to the chimeric transcript fusion point. The reporter probe is coupled to a tag containing a fluorescent barcode that provides the detection signal and identifies the transcript. We analyzed 42 sarcomas: 10 Ewing sarcomas (6 EWS-FLI1 type-1 and 4 type-2); 12 desmoplastic round blue cell tumors (all EWS-WT1), 17 synovial sarcomas (11 SYT-SSX1 and 6 SYT-SSX2) and 3 alveolar rhabdomyosarcomas (2 PAX3-FKHR, 1 PAX7-FKHR). All cases were corroborated by RT-PCR. Twenty-two cases were fresh frozen tissue (FFT) and 20 formalin-fixed paraffin embedded (FFPE). Sensitivity controls consisted of serial dilutions (50%, 25%, 10%, 5%, 1% and 0.5%) of 6 sarcoma cell lines bearing these translocations.

Results: This NanoString assay detected the correct fusion transcript in all 39 tumor samples with satisfactory results and in 6/6 sarcoma cell lines. One of 22 FFT (5%) and 2 of the 20 FFPE samples (10%) gave uninterpretable results due to poor RNA quality. There were no false positives. The technical detection sensitivity ranged from 5-10% tumor in 90-95% normal. The standard assay design cannot discriminate between fusion transcripts with the same 3' fusion partner (e.g. PAX3-FKHR and PAX7-FKHR).

Conclusions: The NanoString Platform is well suited to the multiplex detection of cancer translocation fusion transcripts, requiring no amplification and minimal technical hands-on time. The assay is tolerant of partially degraded RNA and its technical detection sensitivity is suitable for routine diagnostic testing. This is a promising platform for broad screening of cancer translocation fusion transcripts in clinical laboratories.

1902 Validation and Application of New Immunostain Algorithm for Molecular Subtype Classification of Diffuse Large B-Cell Lymphoma (DLBCL): An International DLBCL Rituxan-CHOP Consortium Program Study

JT Malik, et al. R-CHOP Consortium Program, Madison, WI.

Background: Gene expression profiling (GEP) has identified 2 molecular subtypes of DLBCL: germinal center B-cell-like (GCB) and activated B-cell-like (ABC). A new algorithm using 5 immunostains (GCET1, CD10, BCL6, FOXP1 and MUM1) was recently developed (CCR 2009;15:5494). It has yet to be independently validated in a large series of DLBCL patients treated with either CHOP or Rituxan-CHOP.

Design: The purpose of this study is to validate the new algorithm in 315 CHOP treated and 651 Rituxan-CHOP treated DLBCL patients from 20 medical centers, and to correlate with GEP and clinical outcome. Immunostains are performed on tissue microarrays, and semi-quantitative assessments are conducted using the established cut-off values to classify as either GCB or ABC. GEP is performed using U133plus 2 GeneChips (Affymetrix) method in 122 of the cases. Overall survival (OS) and event-free survival (EFS) are analyzed using the Kaplan-Meier method.

Results: Using GEP as the gold standard in 122 of the cases, 93.3% (99/106) are correctly classified into the GCB and ABC subtypes using the new algorithm [table 1]. Application of this algorithm in 315 CHOP treated DLBCL patients predicts 5-year OS (50% in GCB vs. 30% in ABC, p<0.0001) [figure 1]. Application in 651 Rituxan-CHOP treated DLBCL patients also predicts 5-year OS (60% in GCB vs. 45% in ABC, p<0.0001) [figure 2].

Table 1

		CLASSIFICATION BY IHC ALGORITHM		
		ABC	GCB	Total
CLASSIFICATION	ABC	54	3	57
BY	GCB	4	45	49
GEP	Unclassifiable	13	3	16
ANALYSIS	Total	71	51	122

Figure 1

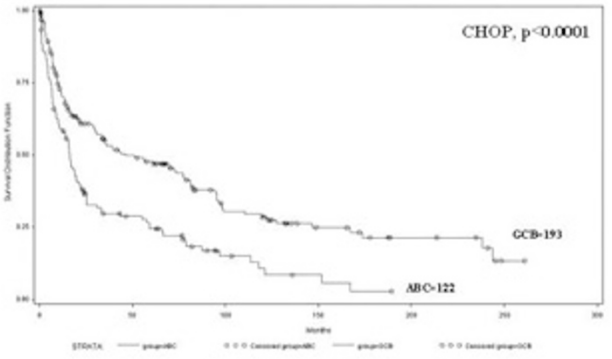

Figure 2

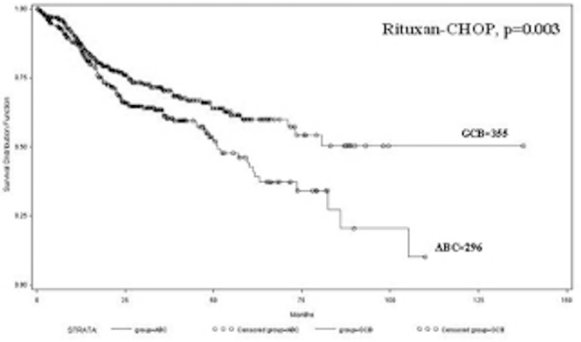

Conclusions: This study confirms an improved accuracy of the new immunostain algorithm for the molecular subtype classification of DLBCL, in patients treated with either CHOP or Rituxan-CHOP. Immunophenotyping significantly correlates with GEP and clinical outcome, thereby enhancing the clinical application of risk stratification in DLBCL patients.

1903 Elucidation of Proteins Involved in the Bortezomib Resistance of Multiple Myelomas though iTRAQ Analysis

J Micallef, J Chen, M Dharsee, S Ackloo, K Evans, H Chang. University Health Network, University of Toronto, Toronto, Canada; Ontario Cancer Biomarker Network, Toronto, Canada.

Background: Multiple myeloma (MM) is a neoplasm of terminally differentiated plasma cells in the bone marrow. Despite advances in clinical care, MM remains an almost universally fatal disease. Bortezomib, a novel proteasome inhibitor represents a promising new clinical strategy for relapsed and refractory MM. However, only 30-40% of MM patients respond to this treatment. The mechanism of resistance is not understood.

Design: In order to gain insights into the mechanism of bortezomib resistance, we examined the differentially expressed proteins between 8226-S (bortezomib sensitive) and 8226-R5 (bortezomib resistant) cell lines using iTRAQ mass spectrometry (MS). The MS based multiple-reaction-monitoring technique (MRM) was then used to independently verify the quantitative differences of the protein expression levels between the two cell lines. RNA interference strategies are being utilized in order to determine the differentially expressed proteins that maybe involved in drug resistance and the associated signaling pathways.

Results: We identified 176 proteins to be differentially expressed between 8226/S and 8226/R5 by iTRAQ mass spectrometry. Among these proteins, 115 (65%) were up-regulated and 61 (35%) were down-regulated. Using a biological systems analysis approach we then identified 36 cancer relevant proteins. From this list, we chose two proteins that may contribute to bortezomib resistance. One such protein is Ubiquilin-4, an ubiquitin-like protein involved in the unfolded protein response which has been shown to protect against cell death. The second protein we chose was MARCKS, a PKC substrate that has been implicated in conferring drug resistance to ovarian carcinoma cells. Differential expression of these proteins between resistant and sensitive cells was verified by MRM and then confirmed by RT-PCR and western blot analysis. Knockdown of these proteins through siRNA techniques is being used to determine their role in MM bortezomib resistant cell lines. Similar strategies will also be used to identify additional proteins that may be involved in drug resistance.

Conclusions: The use of MS based techniques is a powerful tool that will allow us to identify relevant signaling pathways involved in MM drug resistance. Such knowledge will guide the design of additional therapeutic targets and help tailor patient specific treatment.

1904 MicroRNA Expression and Response to Sorafenib, Cytarabine, and Idarubicin in Patients with Acute Myeloid Leukemia

MP Powers, JR Rushton, H Yao, BA Barkoh, D Jones, R Luthra. BCM, Houston, TX; MDACC, Houston, TX.

Background: MicroRNA gene expression has been correlated with mutation status and prognosis in acute myeloid leukemia (AML). AML often has gain of function mutations in the tyrosine kinase FLT3 via either an internal tandem duplication (ITD) or kinase domain point mutation (KD). Sorafenib is a multi-kinase inhibitor which has been shown to target the FLT3 kinase in vitro and has shown promise in treating both FLT3 positive and negative leukemia when combined with the induction agents idarubicin and cytarabine. The molecular correlates of FLT3 response are not yet known. We evaluated the utility of miRNA profiling in identifying responsive AML.

Design: 17 patients treated with IAS (6 responders and 11 non-responders) had total RNA extracted from their diagnostic leukemia sample. 565 miRs were profiled with microarrays (Exiqon) with additional miRs profiled by TaqMan RT-PCR(Applied Biosystems). SAM analysis and the t-test were done on the 129 highest and most variable expressed genes to identify the genes differentially expressed between responders and non-responders and those that correlate with mutations in FLT3 (50% mutated), NPM1 (41% mutated), and CEBPA (29% mutated) mutations and myeloid v. monocytic blast phenotype.

Results: Unsupervised hierarchical clustering revealed miRNA expression patterns segregated primarily based on FLT3 mutation status and were similar to those previously reported (i.e. miR-10 family) but were not associated with IAS response. miR-660 was the most significantly upregulated in the non-responders ($P<0.003$), whereas members of the miRNA-181 family were upregulated in the responders The miR-181 family also correlated with the myeloid blast phenotype and were higher in the CEBPA mutated cases. miR-660 showed a week association with CEBPA mutation status and cellular phenotype.

Conclusions: A higher level of miR-660 expression correlates with the lack of response to IAS in AML patients. Conversely, the miR-181 family was expressed at a higher level in responders and correlated with CEBPA mutation status, a known good prognostic marker, and with the myeloid blast phenotype. Comparisons of markers of response of IAS to IA-alone will allow assessment of the specificity and utility of these miRNA biomarkers in personalized AML therapy.

1905 Glycoproteomic Analysis of Human Lung Adenocarcinomas Using Lectin Glycoarrays and Tandem Mass Spectrometry: Differential Expression and Glycosylation Patterns of Vimentin and Fetuin A Isoforms

MH Roehrl, J-H Rho, JY Wang. Boston Medical Center, Boston, MA; Brigham and Women's Hospital, Boston, MA.

Background: Human lung cancer is a major cause of cancer mortality worldwide. Advances in pathophysiologic understanding and novel biomarkers for diagnosis and treatment are sorely needed. We have undertaken a comprehensive glycoproteomic analysis of human lung adenocarcinoma tissues.

Design: The glycoproteomes from paired human lung adenocarcinoma and normal tissue were biochemically enriched by lectin affinity to Con A, WGA, and AIL followed by 2-D PAGE and tandem mass spectrometric (MS/MS) identification. The chemical and structural alterations at N- and O-linked glycosylation sites were interrogated with high-density lectin glycoarrays and analyzed by computational pattern decomposition.

Results: 2-D PAGE analysis revealed 30 differentially expressed protein spots, from which 15 proteins were identified by MS/MS, including 8 up- (A1AT, ALDOA, ANXA1, CALR, ENOA, PDIA1, PSB1 and SODM) and 7 down-regulated (ANXA3, CAH2, FETUA, HBB, PRDX2, RAGE and VIME) proteins in lung cancer. By RT-PCR, 9 proteins showed positive correlation between mRNA and glycoprotein expression. Vimentin and fetuin A (α_2-HS-glycoprotein) were selected for further investigation. While there was little correlation between total protein abundance and mRNA abundance, expression of Con A-, WGA-, and AIL-captured vimentin protein was consistently decreased in cancer. Lectin glycoarray pattern analysis suggested that vimentin from normal and cancerous lung tissue differ in their contents of sialic acid and GlcNAc. For fetuin A, the correlation between total protein and mRNA abundance showed concordant decrease in cancer. WGA- and AIL-binding fetuin A was also consistently decreased in cancer. Glycoarray analysis suggested that fetuin A glycan structures recognized by Con A were altered in lung cancer, whereas the WGA- and AIL-specific structures were not.

Conclusions: The intriguing expression patterns of different isoforms of glycosylated fetuin A and vimentin in lung cancer illustrate the complexities and benefits of in-depth glycoproteomic analysis. Importantly, mRNA abundance measurements alone fail to capture the chemical diversity of the posttranslationally regulated cancer glycoproteome. The discovery of differentially glycosylated protein isoforms in lung adenocarcinoma may represent avenues towards new functional biomarkers for diagnosis, treatment guidance, and response monitoring.

1906 FusionSeq: A Modular Framework for Finding Gene Fusions by Analyzing Paired-End RNA-Sequencing Data

A Sboner, L Habegger, D Pflueger, S Terry, DZ Chen, AK Tewari, N Kitabayashi, BJ Moss, MS Chee, F Demichelis, MA Rubin, MB Gerstein. Yale University, New Haven; Weill Cornell Medical College (WCMC), New York; WCMC, New York, NY; Prognosys Biosciences, Inc., La Jolla; WCMC, New York; The Broad Institute of MIT and Harvard, Cambridge.

Background: Next-generation sequencing can interrogate genomes and transcriptomes to elucidate driving molecular events, such as gene fusions. One of the newest sequencing technologies, Paired-End (PE) RNA-Sequencing, can detect novel transcript fusions missed by standard techniques.

Design: We developed FusionSeq (http://rnaseq.gersteinlab.org/fusionseq), a platform independent framework consisting of: 1) a mapping module, finding candidate fusions from PE reads joining two genes; 2) a PE-read filtering module, discarding candidates with aberrant insert-size compared to the transcriptome norm and other artifacts, and 3) a junction-sequence module, identifying the specific sequence at the breakpoints. Candidates are ranked by several statistics: SPER (Supportive-PE-reads-per-million mapped Reads), DASPER (Difference between the observed and Analytically calculated expected SPER) and RESPER (Ratio of Empirically computed SPERs), accounting for the number of PE reads supporting the fusion and the corresponding estimation of how "high" this number is.

Results: Results of top candidate fusions from 6 prostate cancers are presented in the table.

Table: Fusion Candidates Based on Type and Ranked Score.

SAMPLE	TYPE	FUSION CANDIDATE	SPER	DASPER	RESPER
580	intra-chromosomal	TMPRSS2-ERG	44.1	44.1	26.4
1700	intra-chromosomal	TMPRSS2-ERG	25.0	25.0	15.0
106	intra-chromosomal	TMPRSS2-ERG	10.2	10.1	4.9
2621	intra-chromosomal	SLC45A3-ERG	2.3	2.1	4.4
580	read-through	ZNF649-ZNF577	6.0	6.0	3.6
106	read-through	AK311452-AK094188	5.9	5.9	2.8
1700	read-through	VMAC-CAPS	4.0	4.0	2.2
1043	read-through	ZNF649-ZNF577	7.1	7.1	2.0
99	inter-chromosomal	NDRG1- ERG	8.0	7.8	1.9

Conclusions: FusionSeq is able to identify known ERG rearrangements as well as their isoforms and has the statistical support to rank fusion candidates.

1907 Isolation of High Quality miRNA from Decalcified, Formalin-Fixed, Paraffin-Embedded Bone Marrow Biopsy Samples

JA Schumacher, ME Salama, P Szankasi, AK Ho, TW Kelley. ARUP Institute for Clinical & Experimental Pathology, Salt Lake City, UT; University of Utah, Salt Lake City, UT.

Background: Decalcified, formalin fixed, paraffin embedded (D-FFPE) bone marrow biopsy samples present a challenge for molecular testing due to nucleic acid degradation. However, the integrity of micro RNA (miRNA) in D-FFPE tissues has not been well characterized. We evaluated the ability to obtain high quality miRNA from D-FFPE bone marrow biopsies that could be quantified by an array-based real time PCR technique.

Design: Thirty three D-FFPE bone marrow biopsy samples from the hematopathology archives (2006-present) were de-identified. Total RNA was extracted using either Qiagen miRNeasy FFPE or Ambion Recoverall™ kits. Absorbance measurements at 280, 260, and 230nm were performed to assess RNA concentration and purity. Following the manufacturer's protocol, total RNA (60-1090 ng) was reverse transcribed and subjected to quantitative RT-PCR to measure 92 miRNAs using the miFinder RT^2 miRNA PCR array from SA Biosciences. Relative expression values were calculated using the $\Delta\Delta C_t$ calculation with data normalized to the average of the geometric mean of 4-housekeeping miRNAs.

Results: Four cases were excluded from analysis due to low RNA yields (<9ng/μL). The remaining 29 cases yielded a mean RNA concentration of 79.4ng/μL (range 12.6-217.9ng/μL), and mean 260/280 ratio of 1.87 (range of 1.7-2.02). The miRNeasy extraction kit yielded the highest quality RNA with a mean 260/230 ratio of 1.64 (range 0.91-2.15; n=23). The Recoverall™ extraction yielded RNA with a mean 260/230 ratio of 0.47 (range 0.2-0.77; n=6). Those cases with average crossing points for 4-housekeeping miRNAs ≤27 cycles were designated as passing QC for the purposes of this analysis. This maximized the number of evaluated miRNAs with crossing points <30 cycles, within the linear amplification range of the assay. Of 29 cases analyzed, 15 met our QC criterion. 2/5 cases (40%) with RNA isolated using Recoverall™ passed QC and 13/24 cases (54%) with RNA isolated using miRNeasy passed QC. As expected, we found that cases where >100ng total RNA was reverse transcribed had higher QC success rates (14/24) (58%) than those using <100ng total RNA (1/5) (20%). QC failures did not correlate with the age of the tissue block. There was a 51.7% QC pass rate for the samples using our QC criterion of ≤27 cycles for the average of the geometric mean of 4-housekeeping miRNAs.

Conclusions: Array-quality miRNA can be obtained from D-FFPE bone marrow biopsy samples.

1908 Frequency of Loss of Heterozygosity (LOH) on Chromosome Arms 1p and 19q and Methylation of O-6-Methylguanine DNA Methyl Transferase (MGMT) Gene in Different Histologic Subtypes and Grades of Gliomas

G Sharma, A Raghunathan, M Cankovic, L Whiteley, JA Gutierrez, D Chitale. Henry Ford Hospital, Detroit, MI.

Background: Loss of heterozygosity (LOH) 1p/19q has been associated with a better overall prognosis in oligodendroglial tumors, but its role in pure astrocytoma is far less important. Methylation of the DNA repair enzyme MGMT renders a subset of malignant gliomas sensitive to therapy with DNA alkylating agents. Molecular testing for LOH 1p19q and MGMT gene has been gradually but widely accepted in clinical practice. We sought to determine frequency of LOH 1p19q and MGMT methylation status (MGMT-M) among different types and grades of gliomas diagnosed and managed at our institution (a metropolitan tertiary care center) over last 3 years.

Design: Between January 2007 and April 2009, 130 cases of gliomas were tested for LOH 1p19q and MGMT-M. DNA was extracted using standard protocol from formalin fixed paraffin embedded tissues containing more than 80% of tumor. 1p19q allelic status was assessed by loss-of-heterozygosity assays in constitutional DNA/tumor DNA pairs by use of microsatellite markers. For MGMT promoter methylation, DNA was first treated with bisulfite followed by MethyLight assay utilizing TaqMan PCR principle.

Results: There were 65 astrocytomas (A) (1 grade1, 12 grade2, 18 grade3, 34 grade4/glioblastoma), 60 oligodendrogliomas (O) (33 grade2, 25 grade3, 2 grade4), 5 oligoastrocytomas (OA) (4 grade2, 1 grade3). Results for LOH 1p/19q and MGMT-M are as follows:

Table 1: Results for LOH 1p19q

Diagnosis	19q loss	1p loss	1p19q loss	Negative	Total
Astrocytoma	5 (7.6%)	10 (15.4%)	2 (3.1%)	48 (73.8%)	65
Oligodendroglioma	4 (6.7%)	3 (5%)	38 (63.3%)	15 (25%)	60
Oligoastrocytoma	1 (20%)	0	0	4 (80%)	5
Total	10 (7.7%)	13 (10%)	40 (30.7%)	67 (51.5%)	130

Table 2: Results for MGMT-M

Diagnosis	MGMT-M Negative	MGMT-M Positive	Total
Astrocytoma	37 (56.9%)	28 (43.1%)	65
Oligodendroglioma	19 (31.7%)	41 (68.3%)	60
Oligoastrocytoma	2 (40%)	3 (60%)	5
Total	58 (44.6%)	72 (55.4%)	130

Conclusions: Based on our series of 130 patients, we conclude that combined LOH 1p19q was significant in oligodendroglioma and was associated with frequent MGMT-M. Combined LOH1p19q was infrequent in astrocytomas and MGMT-M was frequently observed in 86% of high grade astrocytomas (43.1% overall). Oligodendroglial and astrocytic differentiations clearly have different molecular mechanisms and therapeutic targets.

1909 Genomic Characterization of Peritoneal Mesothelioma Reveals Recurrent Loss of 6, 9, and 22 Chromosomal Material

LA Shatat, JA Bridge, Z Gatalica, JM Hagenkord. Creighton University, Omaha, NE; University of Nebraska Medical Center, Omaha, NE.

Background: Malignant mesothelioma is a rare aggressive tumor that arises from serosal surfaces. Peritoneal mesothelioma is four times less common than its pleural counterpart. Previous genomic studies performed on pleural tumors showed deletions of 1p21-22, 3p21, 4q, 6q, 9p21, 13q13-14,and 14q have been repeatedly observed, while monosomy 22 was the most frequent numerical change. However cytogenetic studies of peritoneal mesotheliomas are few.

Design: In an effort to characterize potential genomic alterations in peritoneal mesothelioma, representative peritoneal mesothelioma samples from four male patients (age range 50-73 years) were subjected to both conventional cytogenetic and SNP (single nucleotide polymorphism) array karyotyping analyses. The former was conducted on fresh tissue per standard protocol and the latter on DNA extracted from corresponding formalin-fixed, paraffin-embedded tissue using Affymetrix 250K Nsp arrays. Results were compared to the literature.

Results: Complex numerical and/or structural abnormalities affecting all chromosomes except chromosome 21 were identified using these two complementary methodologic approaches. Loss of all or a portion of the short and long arms of chromosomes 5 and 6, respectively, was seen in 3 of 4 cases. Deletion of chromosomes 9 and 22 were seen in 2/4 cases.

Conclusions: Peritoneal mesotheliomas show complex cytogenetic abnormalities similar to those previously described for pleural-based tumors. Conventional culture based karytoyping and a novel virtual karyotyping using SNP arrays are complementary methods which, when combined, can provide a more targeted analysis of oncogenes and tumor suppressor genes involved in the pathogenesis of peritoneal mesotheliomas.

1910 DNA Copy Number Analysis and Gene Expression Profiles in Abdominal Malignant Mesothelioma (AMM)

AN Sireci, B Levy, RN Taub, JL Chen, O Nahum, AC Borczuk. Columbia University Medical Center, New York, NY.

Background: AMM is a neoplasm of the abdominal serosa with two distinct prognostic subgroups. We describe recurrent genetic abnormalities in this tumor type and identify five that correlate with prognosis.

Design: Gene expression (GE) profiling (Affymetrix U133 Plus2 array) was performed on laser capture microdissected AMM from 14 patients (7 favorable prognosis and 7 poor prognosis, as defined by survival at 1000 days). Needle-dissected tumor from 13 of these patients was studied for copy number (CN) alteration (Affymetrix SNParray 6.0). GE and CN data were analyzed using Partek software. A list of CN alterations present in >35% of tumors, regardless of prognosis, was compiled. Genes with significant CN-GE correlations that predicted prognosis were identified.

Results: A list of 19 genes that exhibited CN variation in >35% of tumors is summarized in table 1 by chromosomal region. BAP1, a known BRCA1-associated tumor suppressor gene, was lost in 5 of 13 tumors. A region of genomic loss in 6/13 cases on 22q11.1 contained BCL2-like13 and BID, two genes with pro-apoptotic functions. Five genes for which CN analysis correlated significantly with GE and that clustered by prognosis were identified. DENND1B, gained in 3/6 poor prognosis tumors and 0/7 of good prognosis tumors is a known anti-apoptotic protein. Additionally, LAMC1, a laminin family member, was gained in 4/6 poor prognosis tumors and remained unchanged in all good prognosis tumors. Over-expression of laminins has been shown in aggressive gliomas.

Table 1: Recurrent CN Losses in 13 AMM

Chromosomal cytoband	Location	# of genes in region	# abnormal	Loss or gain
1q21.3	150.837000 to 150.853200	2 (Lep14, Lep15)	6	Loss
3p21.1	52.3 to 52.6	10 (BAP1, PBRM1)	5	Loss
22q11.1	15.420 to 16.890	19 (BCL2-L13, BID)	6	Loss
22q12.1	26.565 to 26.776	1 (sez6l)	7	Loss
22q21.23	22.655 to 22.727	4 (GSTT1)	5	Loss

Conclusions: We have identified 19 recurrent CN alterations in AMM. Additionally, five genes with copy number variations that correlated with GE and that predicted prognosis were found. Four of these have been implicated in other malignancies.

1911 Enhanced Molecular Characterization of Undifferentiated Tumors: A Series of 10 Cases

SJ Sirintrapun, C Cohen. Emory University, Atlanta, GA; Wake Forest University, Winston-Salem, NC.

Background: CancerTYPE ID integrates expression of 92 genes to distinguish 39 tumors and 64 subtypes.Gene profiles are made extracting mRNA from embedded tissue with RT-PCR.Test gene signatures are compared to a reference database generating a prediction.

Design: Chosen were ten cases with difficult characterization and/or concern for metastases from unknown primaries.Retrospective review was performed by 3 expert pathologists using extensive IHC and clinical correlation.Diagnoses were then compared to predicted type.

Results: CancerTYPE ID further characterized 8/10 cases confirming expert panel diagnoses.

Table1

Site	IHC	Panel Dx	Predicted Type
1Lung	TTF-,Syn+,Chr+,Calci-,S100+,PSA-,CD56+,AE1/3+	Carcinoid	Thyroid Medullary 69%
2Axillary Node	TTF-,ER-,PR-,Her2-,LeuM1-,CK7+,CK20-,AE1/3+	Poorly-Diff CA	Breast 96%
3Bladder and Vagina		Poorly-Diff Squamous CA	Lung Squamous 45%,Skin-Basal-Cell 22%,Leiomyosarcoma 18%
4Cervix		Poorly-Diff CA	Cervix Squamous 91%
5Bowel	TTF-,Syn-,SMA-,Des-,Vim+,WT1-,CD3-,CD20-,CD30-,CD33-,CD43-,CD45-,CD138-,CD21-,CD35-CD31-,CD34-,D2-40-,CD117-,S100-,HMB45-,MelA-,Mel3-,Cam 5.2-,AE1/3-	Undiff Neoplasm,CA or Sarcoma	Soft Tissue MFH 54%
6Neck Node	p53+,PLAP+,CD10-,Syn-,Chr-,S100-,AFP-,HCG-,CD99-,Des-,EBER+,CD3-,CD5-,CD20-,CD43-,CD45-,Cam5.2+,CK LMW-,CK5/6-,CK7+,CK14+,AE1/3+,EMA+	Poorly-Diff CA,Nasopharyngeal or Thymic	Stomach AdenoCA 55%
7Bladder	TTF-,ER-,WT1-,CK7+,CK20-,CDX2-	Clear Cell CA,Bladder or Mullerian	Ovary 56%,Cervix-AdenoCA 38%
8Bladder	p63-,HMWCK-,p504s-,PSA-,PAP-	AdenoCA,Intestinal Type	Bladder 57%
9Bladder		AdenoCA,Intestinal Type	Intestine 99%
10Lung	TTF-,Uroplak-,Thrombomod-,Muci+,CK7+CK20-	Metastatic Bladder CA	Bladder 65%

Two cases had discordance:a lung neuroendocrine tumor(1)predicted as thyroid medullary(calcitonin negative);a lymphoepithelial carcinoma(6)predicted as stomach adenocarcinoma.Correctly predicted were a bladder metastasis to lung(10)and an uncharacterized neoplasm as MFH(5).The urachal adenocarcinoma(9)showed a colorectal molecular profile;bladder squamous carcinoma(3),a lung squamous carcinoma profile.

Conclusions: CancerType ID can serve in adjunct with conventional pathologic evaluation,especially if IHC and/or clinical correlation is not feasible.Use of tissue microdissection and extension of the gene reference database will improve diagnostic use.CancerType ID can also be used in research to provide molecular insight on rare tumors.

1912 Silencing of HPV Viral Oncogenes E6 and E7 in Cervical Cancer

CD Spillane, L Kehoe, O Sheils, CM Martin, JJ O'Leary. Trinity College Dublin, Dublin, Ireland; The Coombe Women and Infant's Univercity Hospital, Dublin, Ireland.

Background: The expression of the HPV oncogenes, E6 and E7, is necessary for the development of cervical cancer. After over 25 years of research many biological activities of E6 and E7 have been established, including their interaction with the major tumour suppressor proteins, p53 and pRb. However, a complete view of their oncogenic potential still eludes us.

Design: In this study, in order to identify downstream cellular targets of the viral oncogenes, short interfering RNA (siRNA) technology was employed to silence E6/E7 oncogenes in HPV16 transformed SiHa cells and subsequently the effect at the cellular transcriptome level was determined using microarray-based gene expression profiling. Five siRNA were designed towards the HPV16 E7 region. TaqMan® PCR specific for E7 and E6, western blotting of E6 and E7 targeted proteins, p53, p21 and Rb, and flow cytometry were applied to examine the effects of the E7 knockdown.

Results: With a concentration of just 10nM four out of five siRNA independently induced in excess of a 70% reduction in RNA levels of E7 and E6. There was also a significant increase in levels of p53, p21 and a decrease in hyperphosphorylated form of pRb indicating a reduction in E6 and E7 protein levels. The introduction of the E7 siRNA into the SiHa cells resulted in a stalling of the cell cycle in the G1 phase, phenotypic changes and an increase in cell autofluorescence, indicating the induction of senescence. Subsequently, the cellular transcriptome of two of the siRNA was assessed by genome-wide microarray analysis. In total 168 genes differentially expressed genes with a fold change values above 2 and FDR below 0.05 were commonly identified on both transcriptome profile. Of the 168 identified genes 158 were down-regulated and 10 up-regulated. A large fraction of these genes are involved in tumor-relevant processes, such as cell cycle regulation, DNA repair and spindle formation.

Conclusions: We describe an RNAi approach which leads to the suppression of HPV16 E6 and E7. This approach, which combines the use of siRNA-mediated gene silencing, microarray screening, and functional classification of differential genes, can be used in functional genomics study to elucidate the role of E6/E7 oncogene in the carcinogenesis of HPV16 and provide some possible targets for clinical treatment and drug development of cervical cancer.

1913 Proteomic Analysis of Pancreatic Duct Fluid: Discovery of Novel Protein Expression in Pancreatic Ductal Adenocarcinoma

CN Thompson, A Sreekumar, VB Bhat, J Ojha, A Cashikar, TG Singh, P Ramalingam, JM McLoughlin, M Shabahang, A Werlang-Perurena, A Rao. Scott & White Hospital/Texas A&M, Temple, TX; Medical College of Georgia, Augusta, GA.

Background: Pancreatic ductal adenocarcinoma (PDAC) usually presents at an advanced stage resulting in significant morbidity and mortality. Currently, there are no clinically useful biomarkers for the detection of occult PDAC. We are using a proteomics-based approach to identify possible PDAC biomarkers.

Design: 25 samples of pancreatic duct fluid (18 PDAC, 7 benign) were analyzed using OFFGEL-based protein fractionation coupled to tandem mass spectrometry. The mass spectrometry data was then searched against the Human IPI sequence database for matches. Synuclein A (SNCA) was one of the proteins elevated in pancreatic adenocarcinoma compared to controls. The expression of SNCA was then correlated to tissue expression by immunoblot and immunohistochemistry. Tissue microarrays were created from 22 archival specimens including 11 cases of PDAC and 11 cases of chronic pancreatitis. The SNCA staining intensity of ductal epithelial cells was graded on a 0-4+ scale.

Results: Thirty proteins were found to have differential expression in pancreatic duct fluid in PDAC compared to controls ($p<0.05$, FDR<10 %). Several of these proteins have been previously reported to be elevated in PDAC. Novel findings included increased expression of SNCA. Immunoblot analysis confirmed elevated levels of SNCA in pancreatic adenocarcinoma tissue compared to controls. Immunohistochemistry demonstrated 2+ diffuse staining of ductal epithelium for SNCA in 9 of 11 PDAC cases with 1+ staining of associated stroma compared to focal, 0-1+ staining in benign ductal epithelium. Strong staining was noted in both benign and tumor acini.

Conclusions: Synuclein A is overexpressed in pancreatic duct fluid and tissues derived from patients with pancreatic adenocarcinoma indicating that this protein may be involved in the pathogenesis of PDAC. Mechanistic understanding of its role in PDAC may reveal prognostically relevant pathways. The differential expression in malignant and benign ducts may also be diagnostically useful.

1914 MicroRNA/Small RNA Profiling Using Frozen and Paraffin Renal Cell Carcinoma Tissue Cohort by Next-Generation Sequencing

L Weng, X Wu, H Gao, B Mu, X Li, J Wang, C Guo, J Jin, M Covarrubias, L Weiss, H Wu. City of Hope, Duarte, CA.

Background: MicroRNA (miRNA) is a group of small non-coding regulating RNAs and has shown altered expression in cancer. Until recently, microarray and real-time PCR have been widely used for quantitative miRNA studies. With the major limitations in test specificity and capability of detecting unknown miRNA and other small RNA targets, they are being replaced by the newly developed next-generation sequencing technology. Although next-generation sequencing has been recently used to study miRNA/small RNA expression in cancer primary cell culture or cell lines and shown great potential, similar studies applied to human cancer tissue cohorts have not been reported. Specifically, FFPE samples have not been used for small RNA studies by next-generation sequencing, since it has been assumed to have insufficient quality of RNA. However, clinical tissue samples are routinely stored as FFPE samples. Therefore, establishing a method to use FFPE samples for miRNA expression profiling by deep sequencing would make future clinical cohort/trial-based studies possible.

Design: (1) A clear cell renal cell carcinoma (CCRCC) cohort with both frozen and corresponding FFPE samples was established. It included frozen tissue from 3 benign kidney and 3 CCRCC samples, and their FFPE counterparts. (2) Deep sequencing of small RNA in all samples using Illumina GAII was performed. (3) Microarray testing on all frozen samples was performed using an Agilent MicroRNA Array. (4) The miRNA expression level of each sample was compared between deep sequencing and microarray platforms. (5) miRNA/small RNA expression was profiled in both frozen and FFPE cohort sets and the results were compared.

Results: (1) miRNAs and other small RNAs can be detected by deep sequencing in frozen samples, and the expression level of miRNAs is highly correlated with that measured by microarray. (2) Differentially expressed miRNAs identified in deep sequencing highly correlated with the microarray and with real-time PCR results. (3) miRNA and other small RNAs can be detected by deep sequencing in FFPE samples, and the expression levels of miRNA are highly correlated between frozen and FFPE sample pairs. (4) Differentially expressed miRNAs identified in FFPE and frozen samples with deep sequencing are highly similar.

Conclusions: (1) Deep sequencing platform can be used for human tissue cohort studies to profile miRNA/small RNA expression in cancer. (2) A FFPE tissue cohort can be used reliably to profile miRNA expression in cancer.

1915 The Detection of EGFR Mutation Status with Immunocytochemistry in Circulating Tumor Cells Using Mutation Specific Antibodies

J Yu, CH Hu, DQ Li, XM Zhou, MJ Comb. Cell Signaling Technologg, Danvers, MA; The Second Xiangya Hospital, Central South University, Changsha, Hunan, China; The Second Xiangya Hospital, Changsha, Hunan, China.

Background: The somatic mutations in the EGFR gene are found in a subset of lung cancer and are associated with sensitivity to the EGFR tyrosine kinase inhibitors (TKI). Detecting the gene mutations or mutant protein has provided clinicians useful information for the selection of the treatment to this subset of lung cancer patients. The purpose of this study is to develop a fast and reliable clinical assay to detect the status of EGFR mutations without patient tumor tissue.

Design: We used fluorescence immunocytochemistry with mutation-specific antibodies in circulating tumor cells (CTC) or the cells from pleural effusion. This assay detects the proteins of most common EGFR mutations, exon 19 deletion and L858R point mutation, which represent about 90% of EGFR mutations in NSCLC.

Results: We used NSCLC cell lines to verify that the mutation-specific antibodies can specifically detect EGFR mutations and the EpCAM antibody was selectively labeled at the epithelial cells by fluorescence immunocytochemistry.

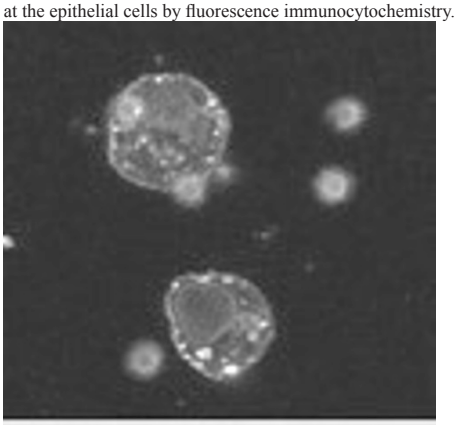

Next, we tested the cancer cell lines enriched from mixed with blood.

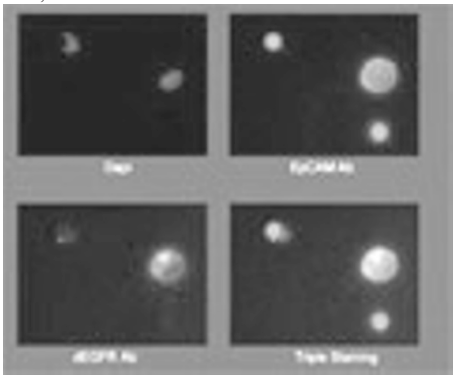

Finally, we confirmed the assay from the cells recovered from the blood or pleural effusion of late stage NSCLC patients.

Conclusions: Fluorescence immunocytochemistry with mutation-specific antibodies to detect EGFR mutations on the tumor cells from blood or pleural effusion is a reliable, easily accessible and cost efficient assay for patient selective to target therapy, especially in the late stage NSCLC patients without tumor tissue or the patients treated by TKI for following up the response.

1916 Protein Expression Profiling of Irinotecan Pathway in Lung Cancer

W Zhang, WS Zhang, EL Lee, HL McLeod. Howard University Hospital, Washington, DC; The Second Hospital of Nanjing, Nanjing, Jiangsu, China; UNC School of Pharmacy, Chapel Hill, NC.

Background: The exact mechanism for variation of response to chemotherapy remains unclear. Individualized therapy strategies for cancer will require a more thorough understanding of the pathways influencing drug fate, including expression of cellular target enzymes, metabolism enzymes and cellular transporters. Irinotecan is an excellent example of an anticancer drug in need of individualization. We profile expression of proteins in an irinotecan pathway in lung small cell carcinoma and non-small cell carcinoma tissues and construct a new pharmacologic pathway to help advance individualization in the selection of cancer therapy.

Design: Paraffin embedded tumor tissues from 15 patients with lung small cell carcinoma, 49 patients with stage IV non-small cell carcinoma (21 squamous cell carcinoma, 18 adenocarcinoma and 10 undifferentiated large cell carcinoma) were used to construct a tissue microarray. Fifteen markers, including CES2, NFkappaB, XRCC1, CDC45, TDP1, TOP1, PARP1, ABCC1, ABCC2, ABCC3, ABCB1, ABCG2, p53, ERCC2, UGT1A1, that are related to the irinotecan pathway were immunohistochemically stained on the tissue microarray. Protein expression was assessed to derive an overall expression level. Hierarchical clustering was used with unsupervised algorithms to identify patterns of protein expression that produced distinct clusters of patients.

Results: The relative expression levels across the 15 pathway proteins and the interpatient variability were considerable. Using hierarchical clustering, 4 protein clusters and 3 patient groups had highly similar indices based on the protein expressions. Protein expression of this drug pathway is not associated with lung carcinoma histological type. Cluster analysis identified a variety of histological types with the same pharmacological profile. The 3 patient groups had no unique clinical pathologic features but could be differentiated by the statistically significant differences in the protein expression levels of 5 proteins.

Conclusions: Gene expression profiling could be valuable for predicting tumor response to chemotherapy and for tailoring therapy to individual cancer patients. Establishing the ability of pathway analysis to discern patient populations who have a high likelihood of benefit from a given chemotherapy agent or those who will receive no benefit will provide the basis for selection of therapy for individual patients.

1917 Discovering Multivariate Gene Expression Markers for Relapse Prediction in Pediatric Acute Lymphoblastic Leukemia

Y Zhou, D Dziuda. New York Medical College, Valhalla, NY; Central Connecticut State University, New Britain, CT.

Background: Identification of cancer patients with high risk of treatment failure is becoming an important aspect of pathology practice. Discovery of reliable predictive and prognostic markers using high content gene expression profiling or genome analysis have proven both promising and challenging. Oncogenesis is a result of heterogeneous signaling dysregulation converged on critical cellular functions. The goal in discovery of predictive and prognostic marker is to identify a minimal set of genes or proteins that has maximal discriminating power to separate phenotypic classes, and reveals the underlying mechanism contributing to the phenotypic differences.

Design: We describe a supervised multivariate biomarker discovery approach utilizing stepwise selection driven by a well-defined measure of discriminatory power (the Lawley-Hotelling T 2 metric), which (i) allows for identification of a set of genes whose joint expression pattern efficiently discriminate phenotypic classes, (ii) facilitates biological interpretation of underlying dysregulations. This approach is illustrated on prediction of relapse in pediatric B-cell acute lymphoblastic leukemia (B-cell ALL) using publicly available gene expression data sets.

Results: Based on a cohort of B-cell ALL with mixed subtypes of cytogenetic changes, a set of genes, less than 20, was identified as a multivariate biomarker for predicting the risk of disease relapse. This marker is then tested on another independent set of B-cell ALL, and predicts disease relapse with 91% sensitivity. Ensemble of the biomarker reveals gene expression pattern that is associated with the relapse risk in B-cell ALL.

Conclusions: We demonstrate the usefulness of multivariate approach in identifying a small set of prognostic marker. The marker contains sufficiently small numbers of genes that can be readily converted to RT-PCR based assays.

Techniques

1918 Biospecimen Inventory and Operations System (BIOS) for Management of Annotated Tissue Bank Specimens for Anatomical Pathology

W Amin, G Greenwood, M Bisceglia, L Mock, R Dhir, AV Parwani. University of Pittsburgh, Pittsburgh, PA; University of Pittsburgh Medical Center, Pittsburgh, PA.

Background: There is a need for tools that provide researchers access to highly annotated biospecimens for research. The Biospecimen Inventory and Operations System is an enterprise biorepository system designed for a high-quality, well annotated biospecimen management for clinician and researchers need. It provides a robust query capability that eventually allows biomarkers to identify the biospecimens as per the need of the research community.

Design: BIOS is a Microsoft .NET web application with a SQL Server database. It unifies the efforts of tissue collection, patient consents status, billing and data aggregation in one module. It links to Medipac for accurate importing of patient demographics. It will pull patient mapped data automatically through integration with lab information systems and synoptics and other institutional electronic data sources, from hospital information systems.

Results: The BIOS system has been successfully implemented at our institute and is currently being used for the day to day operations of a system-wide tissue bank. BIOS provides a central repository for the tissue bankers for tracking and distribution of biospecimens and for robust querying and reporting of biospecimens and associated data to fulfill the requirements of clinical translational researchers. By combining the flexible query interface of BIOS with the ability to export the result of queries, the tissue bankers will be able to prepare virtually any custom report they require, from summaries of bank-wide operations during a specified period to daily work lists for a particular banker.

Conclusions: BIOS in provides a central biorepository to access information on multimodal data sets and the ability for tracking and integration with other limbs of a tissue bank. In addition BIOS provides the tissue bankers with a robust, queryable, and maintainable system that can be integrated with other tissue banking and pathology tools including image and molecular data integration. Furthermore, this model can be successfully deployed at other institutions.